Transparent Conductive Two-Dimensional Titanium Carbide Epitaxial Thin Films

Joseph Halim[†‡§], Maria R. Lukatskaya[†‡], Kevin M. Cook[†‡], Jun Lu[§], Cole R. Smith[†], Lars-Åke Näslund[§], Steven J. May[†], Lars Hultman[§], Yury Gogotsi[*†‡], Per Eklund[*§], and Michel W. Barsoum[*†§]

[†] Department of Materials Science & Engineering, Drexel University, Philadelphia, Pennsylvania 19104, United States

[‡] A.J. Drexel Nanomaterials Institute, Drexel University, Philadelphia, Pennsylvania 19104, United States

[§] Thin Film Physics Division, Department of Physics, Chemistry and Biology (IFM), Linköping University, SE-581 83, Linköping, Sweden

Abstract

Since the discovery of graphene, the quest for two-dimensional (2D) materials has intensified greatly. Recently, a new family of 2D transition metal carbides and carbonitrides (MXenes) was discovered that is both conducting and hydrophilic, an uncommon combination. To date MXenes have been produced as powders, flakes, and colloidal solutions. Herein, we report on the fabrication of ~1 × 1 cm2 Ti_3C_2 films by selective etching of Al, from sputter-deposited epitaxial Ti_3AlC_2 films, in aqueous HF or NH_4HF_2.
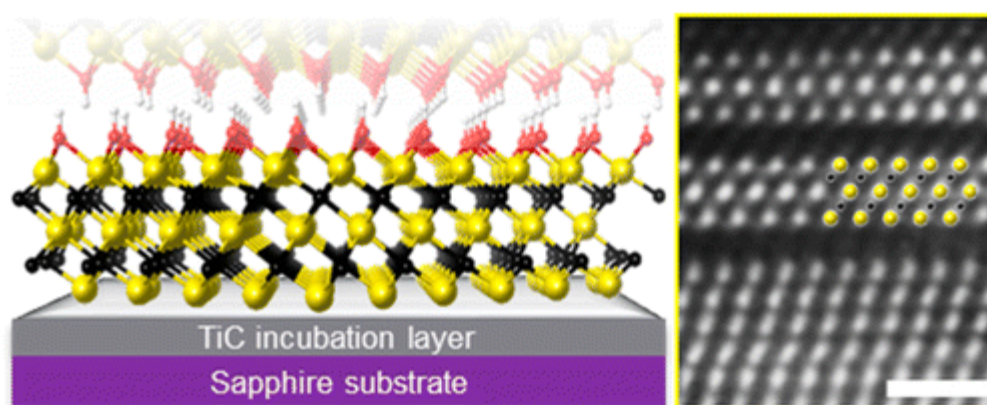
Films that were about 19 nm thick, etched with NH_4HF_2, transmit ~90% of the light in the visible-to-infrared range and exhibit metallic conductivity down to ~100 K. Below 100 K, the films' resistivity increases with decreasing temperature and they exhibit negative magnetoresistance—both observations consistent with a weak localization phenomenon characteristic of many 2D defective solids. This advance opens the door for the use of MXenes in electronic, photonic, and sensing applications.

Introduction

Since the discovery of graphene,[1-3] two-dimensional (2D) solids have attracted considerable attention due to the unique properties bestowed upon them by their reduced dimensionality. These

are currently being considered for a multitude of applications, including electronic, photonic, and energy storage devices.[4-6] For instance, graphene has an electron mobility of 2×10^5 cm^2 V^{-1} s^{-1} at room temperature, which shows a weak dependence on temperature.[3, 7] Furthermore, a single layer of graphene transmits 97.7% of light in the near-infrared to ultraviolet range.[8] This combination of unique electronic and optical properties has positioned graphene as a promising material for transparent conductive electrodes.

The immense interest generated by graphene has renewed efforts to identify and characterize other 2D solids such as BN,[9] MoS$_2$[10, 11] that may possess equally attractive properties. Recently, we discovered a new family of 2D materials that is both metallically conducting and hydrophilic, an uncommon combination indeed. This new family of materials was labeled MXenes[6, 12] to emphasize that they are produced by selective etching of the A layers from the MAX phases and their similarity to graphene.[13] The latter are a large family of more than 60 phases, with the general formula of $M_{n+1}AX_n$, where n = 1, 2, 3, where M is an early transition metals, A is an A-group (12–16) element, and X is carbon and/or nitrogen.[14] The MAX phases are nanolaminated, wherein every n-layers of M atoms are interleaved with layers of pure A; the X atoms occupy the octahedral sites between the M atoms. To date the following MXenes have been synthesized: Ti$_3$C$_2$,[13] Ti$_2$C, Ta$_4$C$_3$, TiNbC, (V$_{0.5}$,Cr$_{0.5}$)$_3$C$_2$, Ti$_3$CN,[15] and most recently Nb$_2$C and V$_2$C.[16]

By varying the M and X elements, as well as the surface chemistries and/or the number of layers, n, in $M_{n+1}X_n$, it is possible to tune the MXene properties. This wealth of new 2D materials has launched experimental and theoretical activities worldwide[17, 18] (see ref 12 for a recent review). MXenes show promise as anodes for lithium ion batteries; a result supported by ab initio calculations.[19-21] More recently, Lukatskaya et al.,[22] have shown that a host of cations (Na$^+$, Mg^{2+}, Al^{3+}, NH$_4^+$, etc.) can be readily intercalated, from aqueous solutions, between the Ti$_3$C$_2$ layers. Volumetric capacitances exceeding 300 F/cm^3 were reported. These values are much higher than those of porous carbon currently used in electrochemical capacitors.

However, thin films are needed to explore electronic or photonic applications. Herein, we report on the synthesis of ~1 × 1 cm^2 epitaxial Ti$_3$C$_2$ thin films. The materials described here represent a substantial advance in several ways: (1) they are produced as continuous epitaxial thin films; (2) in all previous studies, the etchant was hydrofluoric acid (HF). Here, it is shown that ammonium bifluoride, NH$_4$HF$_2$, can be used instead; (3) the one-step synthesis of a MXene, intercalated with ammonia, is demonstrated; (4) the availability of epitaxial films on transparent and insulating sapphire substrates enabled the measurement of some of the fundamental physical properties, such as optical absorption, in a broad wavelength range, and the temperature dependence of conductivity and magnetoresistance down to 2 K. These films show high transparency for wavelengths in the visible to infrared range.

Methods

Deposition of Ti$_3$AlC$_2$

The Ti$_3$AlC$_2$ thin films were deposited from three elemental targets (Ti, Al, and C with diameters of 75, 50, and 75 mm, respectively) using DC magnetron sputtering in an ultrahigh vacuum system described elsewhere.[38, 39] The sputtering process gas was Ar (99.9999% purity) at a constant pressure of 4.8 mbar. The substrates were c-axis-oriented sapphire, Al$_2$O$_3$ (0001), with surface areas of 10 × 10 mm^2 and thicknesses of 0.5 cm (MTI Corp. CA). Prior to deposition, the substrates were cleaned using acetone, rinsed with isopropanol, dried by nitrogen gas, and finally preheated inside the deposition chamber at 780 °C for 60 min. Deposition was performed at 780 °C. Titanium and

carbon targets were ignited for 5 s followed by the ignition of the aluminum target. This procedure resulted in the formation of a TiC (111) incubation layer 5–10 nm thick followed by the growth of Ti_3AlC_2. Previous work have shown that a TiC incubation layer facilitates the growth of epitaxial Ti_3AlC_2.(29, 38, 40)

Synthesis of Ti_3C_2

Two chemicals were used to etch, at room temperature, the Ti_3AlC_2 films. The first was 50% concentrated HF (Sigma Aldrich, Stockholm, Sweden). Samples of nominal thickness of 15, 28, 43, and 60 nm were etched for 10, 15, 60, and 160 min, respectively. The second was 1 M NH_4HF_2 (Sigma Aldrich, Stockholm, Sweden). Samples of the same thickness as those mentioned above were etched for 150, 160, 420, and 660 min, respectively. After etching, the samples were rinsed in deionized water, then in ethanol.

Chemical and Morphological Characterization

X-ray diffraction (XRD) of the films was performed using an X'Pert Powder diffractometer (PANalytical, Almelo, The Netherlands), with a θ–2θ continuous scan of a step size with 0.017° and 40 s dwell time. XRD of the $Ti_3C_2T_x$-IC powders and deintercalated $Ti_3C_2T_x$ thin films were carried out using a diffractometer (SmartLab, Rigaku, Tokyo, Japan) with a θ-2θ continuous scan of a step size of 0.02° and 1 s dwell time.

X-ray reflectometry (XRR) continuous scans were performed using an X'Pert Powder diffractometer (PANalytical, Almelo, The Netherlands), with a step size of 0.01° and 1.76 s dwell time. Simulation for the XRR results was carried out using the X'Pert Reflectivity software produced by PANalytical B.V.

To characterize the chemical states of elements in the thin films before and after etching, X-ray photoelectron spectroscopy (XPS) was performed using a surface analysis system (Kratos AXIS Ultra DLD, Manchester, U.K.). Monochromatic Al Kα X-rays irradiated the samples at an angle of 45°, with respect to the surface; X-ray spot size was 300 × 800 μm. The electron energy analyzer accepted the photoelectrons perpendicular to the sample surface with an acceptance angle of ±15°. The high-resolution spectra were recorded using a pass energy of 20 eV and a step size of 0.1 eV. To avoid broadening of the XPS spectra caused by sample charging, an electron flood gun was used while recording the data. The binding energy scale of all XPS spectra was therefore referenced to the Fermi level which was set to a binding energy of 0 eV. Peak assignments of the spectra were supported through an analysis of a TiC bulk sample of known stoichiometry (1:1) and a TiO_2 thin film of known stoichiometry (1:2). The quantification and peak fitting were carried out using CasaXPS Version 2.3.16 RP 1.6.

Transmission electron microscopy (TEM) imaging, film thickness measurement, and selected area electron diffraction (SAED) acquisition was carried out using a TEM (FEI Tecnai G2 TF20 UT) operated at 200 kV with a point resolution of 0.19 nm. High-resolution scanning TEM imaging (HR STEM), and energy-dispersive X-ray spectroscopy (EDX) were performed using a HRTEM instrument (FEI image/probe double C_s corrected Titan[3] G2 60–300, Eindhoven, The Netherlands) operated at 300 kV with an ultrathin window silicon drift detection X-ray energy-dispersive spectrometer and a monochromator.

Cross-sectional TEM samples were prepared by sandwiching two cross-sectioned samples in a Ti grid that was in turn mechanically polished down to 70 μm, followed by ion milling to electron transparency. Scanning electron microscopy (SEM) (Zeiss Supra 50VP, Germany) was used to investigate the morphology of the Ti_3AlC_2 and $Ti_3C_2T_x$ films.

Optical and Electrical Characterization

Transmittance values of the films were obtained using a spectrophotometer (Perkin-Elmer Lambda 950 UV–vis) with a 2-nm slit width and resolution. Spectra were corrected with both 100% and 0%

transmittance background spectra. A bare sapphire substrate was used as a reference. The number of MXene layers obtained for Figure 3b were calculated by dividing the total film thicknesses by $c/2$, where c is the lattice parameters obtained from XRD.

Room-temperature resistivities were measured using a four-point probe method. Three sheet-resistance measurements were taken for each sample. The errors reported in Table 1 and Supporting Information Table S4 were calculated from these three measurements. The resistivity was obtained by multiplying the sheet resistance with the corresponding average film thickness.

The temperature-dependent in-plane resistivity measurements were performed in a Physical Property Measurement System (Quantum Design, San Diego) using an external current source (Keithley 6220, Ohio) and a nanovoltmeter (Keithley 2182A). A linear four-point probe geometry was used. Gold wires were attached to the films using silver paint. Positive and negative currents were applied at each temperature to eliminate any thermal offsets. The magnetoresistance, MR, measurements were performed with the magnetic field—up to 10 T—applied out of the plane of the film.

Results and Discussion

The films used were 15 to 60 nm thick Ti_3AlC_2 films deposited onto sapphire (000l) substrates by magnetron sputtering. More details can be found in Supporting Information Section I. Scheme 1a shows the process starting from the sputter-deposition of Ti_3AlC_2 (with initial formation of a TiC incubation layer). This is followed by etching of the Al layers resulting in 2D $Ti_3C_2T_x$ layers (Scheme. 1b), where T_x stands for the surface −O, −OH, or −F terminations resulting from the aqueous HF etchant. In Scheme 1b, the Ti_3C_2 surfaces are presumed to be OH-terminated. STEM image of the interface between the TiC incubation layer and $Ti_3C_2T_x$ is shown in Scheme 1c. The fact that the very first MXene layer has an ordered structure bodes well for the production of single layer MXene films.
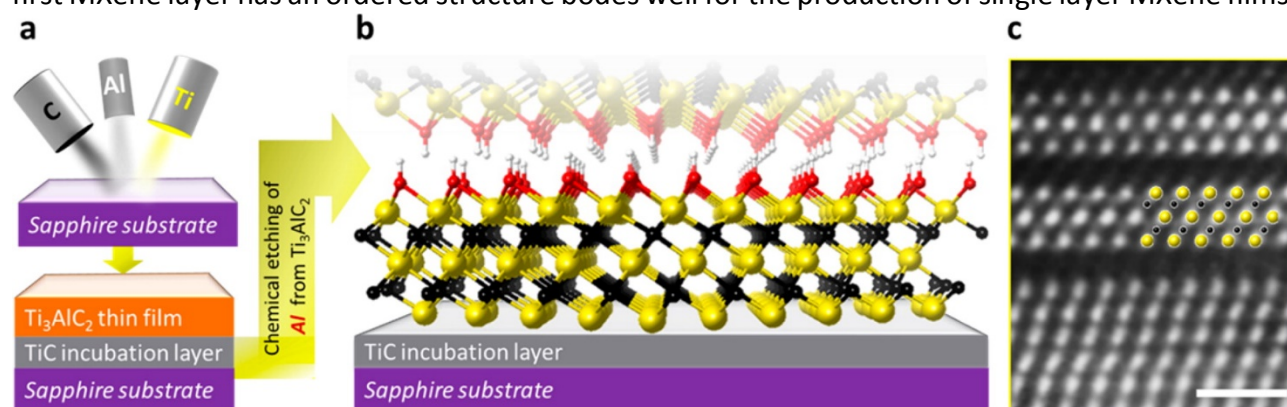
Scheme 1. Steps Used to Produce Epitaxial MXene Films[a]

[a](a) Magnetron sputtering of Ti, Al and C forming a few-nanometer TiC incubation layer on a (0001) sapphire substrate, followed by the deposition of Ti_3AlC_2; (b) schematic diagram of OH-terminated Ti_3C_2 after selective etching of Al from Ti_3AlC_2 (Ti atoms are yellow, C atoms are black, O atoms are red, and H atoms are white); (c) STEM image of the first two $Ti_3C_2T_x$ layers after applying Wiener filter; scale bar is equal to 1 nm. Inset shows Ti atoms in yellow and C atoms in black.

To date, the only etchant reported for producing MXenes has been HF.[13, 15, 16] Herein, we show that, NH_4HF_2 can be used for the same purpose. The main advantage of the latter is that it is less hazardous than HF[23] and is a milder etchant. Its use leads to the concomitant intercalation of

cations during the etching process. For the sake of brevity, these films will be referred to as Ti$_3$C$_2$T$_x$-IC, where the IC represents the intercalated species, viz. NH$_3$ and NH$_4^+$ (see below).

A typical XRD pattern of an as-deposited Ti$_3$AlC$_2$ film (Figure 1a, I) shows the (000l) peaks from Ti$_3$AlC$_2$, a TiC incubation layer) and the sapphire substrate.(23) The presence of only peaks corresponding to basal-plane oriented Ti$_3$AlC$_2$ indicates epitaxial growth, a fact also confirmed by TEM and SAED (Figure 2a). The Ti$_3$C$_2$T$_x$ XRD pattern (Figure 1a, II) on the other hand, shows a shift to a lower angles of the 000l peaks corresponding to an increase in the c lattice parameter from 18.6 Å for Ti$_3$AlC$_2$ to 19.8 Å for Ti$_3$C$_2$T$_x$. The latter value agrees with previous work on Ti$_3$C$_2$T$_x$ synthesized from Ti$_3$AlC$_2$ powders.(13) The XRD pattern of Ti$_3$C$_2$T$_x$-IC (Figure 1a, III), is similar to the other two, except that now c is further increased to 24.7 Å.
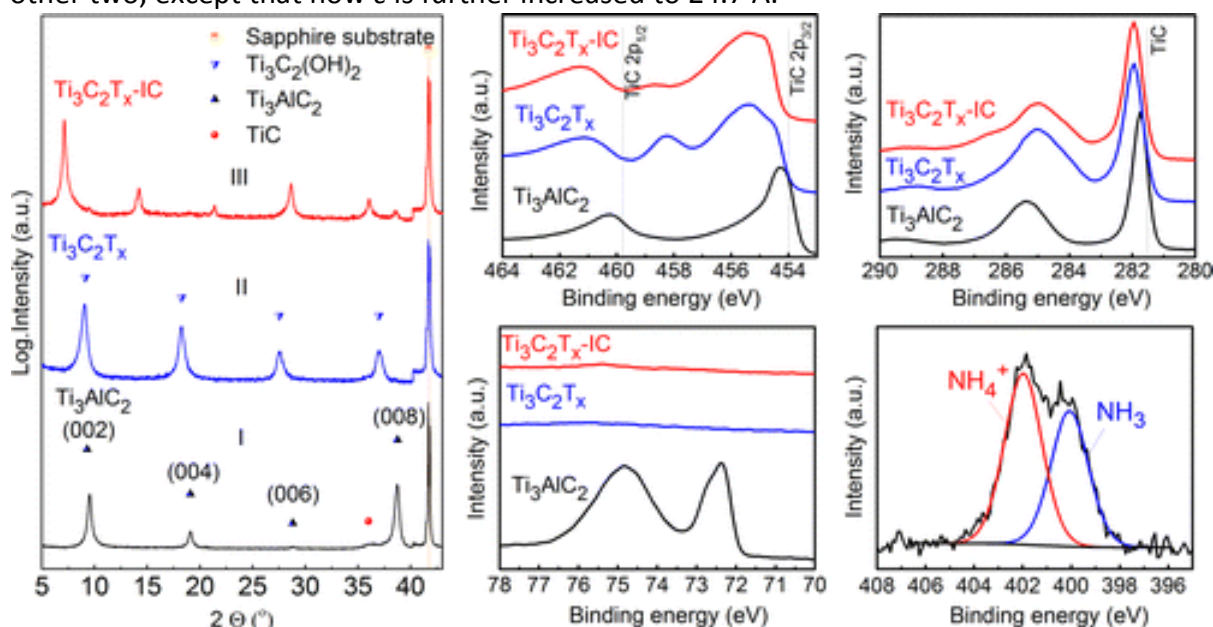

Figure 1. (a) XRD patterns of as-deposited −60 nm nominal thickness - Ti$_3$AlC$_2$ thin films (I), Ti$_3$C$_2$T$_x$ after etching in 50% HF for 2 h 40 min (II), and Ti$_3$C$_2$T$_x$-IC after etching in 1 M NH$_4$HF$_2$ for 11 h (III). XPS spectra of, (b) Ti 2p, (c) C 1s, and (d) Al 2p for Ti$_3$AlC$_2$, Ti$_3$C$_2$T$_x$, and Ti$_3$C$_2$T$_x$-IC thin films, respectively. The vertical lines in panels b and c indicate the positions of Ti (3/2p and 1/2p) and C (1s) binding energies in TiC, respectively. (e) High resolution XPS spectra for N 1s region for Ti$_3$C$_2$T$_x$-IC, best fitted by symmetric Gaussian–Lorentzian curves resting on a Shirley background. The two components correspond to (NH$_4^{+1}$)(24) and (NH$_3$).(25)
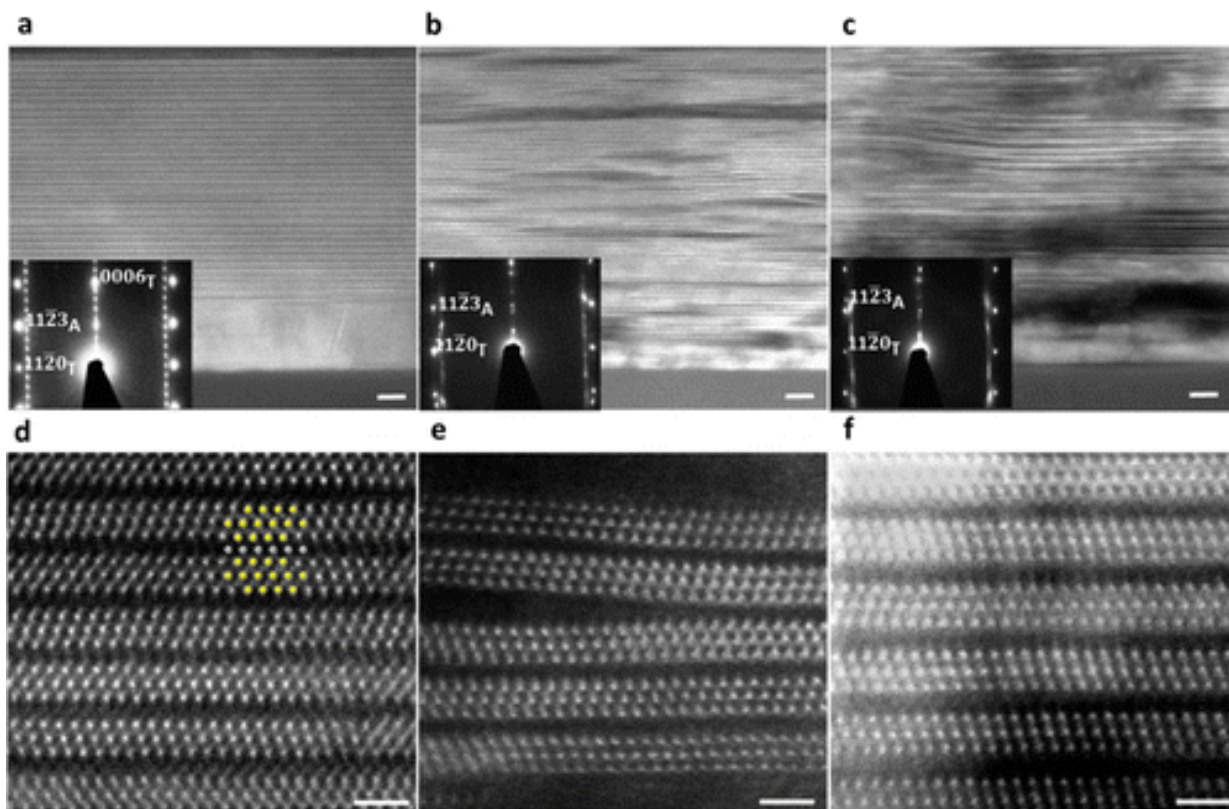
Figure 2. Cross-sectional STEM images of (a) Ti_3AlC_2, (b) $Ti_3C_2T_x$, (c) and $Ti_3C_2T_x$-IC films (60 nm nominal thickness) grown on a sapphire substrate with a TiC incubation layer. Insets show SAED of the film and the substrate. The subscripts A and T correspond to Al_2O_3 and Ti_3AlC_2, respectively. High-resolution STEM images of (d) Ti_3AlC_2, (e) $Ti_3C_2T_x$, and (f) $Ti_3C_2T_x$-IC films along the [$11\bar{2}0$] zone axis. The inset in panel d shows Ti, Al, and C atoms in yellow, gray, and black, respectively. Scale bars for low resolution (a, b, and c) and high-resolution (d, e, and f) images correspond to 5 and 1 nm, respectively.

Similar behavior was observed when Ti_3AlC_2 powders were intercalated with NH_4OH or NH_4F after HF etching. In both cases, the c lattice expansion was of the order of 25% (see Supporting Information Figure S5a). The independence of the increase in the c lattice parameter on the nature of the anion of the etching solution strongly suggests that the cations (NH_4^+) and/or (NH_3), and not the anions, are the intercalated species. We note in passing that the present work is in contradistinction to the recent work by Lukatskaya et al. who intercalated NH_4OH into $Ti_3C_2T_x$,[22] in a two-step process. Herein, the etching and intercalation occur in a single step. This is an important result because it considerably simplifies the intercalation process.

The XPS results, shown in Figure 1b–d for films, with a nominal thickness of 60 nm, demonstrate a shift in the Ti 2p and C 1s (Figure 1b and c) toward higher binding energies for the titanium carbide species in Ti_3AlC_2, $Ti_3C_2T_x$, and $Ti_3C_2T_x$-IC, compared to those of binary TiC (shown in Figure 1b and c as thin vertical lines), indicating the change in the nature of bonding between the Ti and C atoms in Ti_3AlC_2 and the corresponding MXenes. The latter most likely occurs because valence electrons are withdrawn from the Ti atoms, and subsequently from the C atoms, in the MXene layers by the surface functional groups, as well as from the interaction of the surface with the intercalated compounds. The removal of Al is verified by the high-resolution spectra in the Al 2p region for $Ti_3C_2T_x$ and $Ti_3C_2T_x$-IC (Figure 1d), in which a very weak Al signal—most probably originating from aluminum

fluoride (see Supporting Information section I)—is recorded. The Ti$_3$AlC$_2$, Al 2p signal corresponds to Al bonded to Ti, as well as, to surface aluminum oxide.

The reactions of HF with Ti$_3$AlC$_2$ have been postulated by Naguib et al.[15] to be

$$Ti_3AlC_2 + 3HF = AlF_3 + 3/2H_2 + Ti_3C_2 \quad (1)$$
$$Ti_3C_2 + 2H_2O = Ti_3C_2(OH)_2 + H_2 \quad (2)$$
$$Ti_3C_2 + 2HF = Ti_3C_2F_2 + H_2 \quad (3)$$

Reaction 1 is followed by reactions 2 and 3, which result in OH and F terminated Ti$_3$C$_2$ surfaces or Ti$_3$C$_2$T$_x$. The elemental ratio obtained from the analysis of high-resolution (XPS) spectra is Ti$_3$C$_{2.2}$O$_2$F$_{0.6}$ (see Supporting Information section II). As indicated by XPS, terminal hydroxyl and fluoride groups exist on the surface of the material, thereby indirectly confirming the aforementioned reactions. EDX mapping in the TEM (Supporting Information Figure S7) also confirms the presence of F and O atoms between the Ti$_3$C$_2$ layers.

As discussed above for the NH$_4$HF$_2$ etched Ti$_3$AlC$_2$, the etching of the Al and the intercalation of ammonium species occur concomitantly. It is thus reasonable to conclude that in this case the following reactions are operative:

$$Ti_3AlC_2 + 3NH_4HF_2 = (NH_4)_3AlF_6 + Ti_3C_2 + \frac{3}{2}H_2 \quad (4)$$
$$Ti_3C_2 + aNH_4HF_2 + bH_2O = (NH_3)_c(NH_4)_dTi_3C_2(OH)_xF_y \quad (5)$$

Unlike HF etching, NH$_4$HF$_2$ etching results in formation of (NH$_4$)$_3$AlF$_6$ according to reaction 4 (see Supporting Information section III). Reaction 5 depicts the intercalation of NH$_3$ and NH$_4^{+1}$ between the Ti$_3$C$_2$T$_x$ layers.[26] In order to confirm the nature of the intercalating species in Ti$_3$C$_2$T$_x$-IC, a high-resolution XPS spectrum of the N 1s region was recorded (Figure 1e). The latter was best fitted by two components: one for NH$_4^{+1}$ (55.8% of N 1s; peak position, 402 eV; fwhm, 1.8 eV);[24] the other for NH$_3$ (44.2% of N 1s; peak position, 400.1 eV; fwhm, 1.8 eV).[25] It is thus reasonable to conclude that both species intercalate this MXene. We note in passing that both NH$_3$ and NH$_4^+$ intercalate between the 2D layers of transition metal dichalcogenides, such as TiSe$_2$ and TiS$_2$.[27, 28]

The elemental ratio obtained from the analysis of high-resolution XPS spectra (see Supporting Information section II) of Ti$_3$C$_2$ produced by NH$_4$HF$_2$ etching is Ti$_3$C$_{2.3}$O$_{1.2}$F$_{0.7}$N$_{0.2}$. Here again, the XPS analysis indicates the presence of terminal hydroxyl and fluoride groups.

Cross-sectional scanning TEM micrographs of as-deposited Ti$_3$AlC$_2$ films, before (Figure 2a and d) and after etching with HF (Figure 2b and e) or NH$_4$HF$_2$ (Figure 3c and f) clearly show the presence of the TiC incubation layers and the effects of etching on the microstructures of the films. The SAED patterns confirm the out-of-plane epitaxial relationship Ti$_3$AlC$_2$(0001)//TiC(111)//Al$_2$O$_3$(0001).[29] At 18.6 Å, the c lattice parameter for Ti$_3$AlC$_2$, obtained from the SAED pattern and TEM micrographs (see Supporting Information section VIII), is in excellent agreement with that calculated from XRD (18.6 Å). At 19.5–20 Å, the c lattice parameters of Ti$_3$C$_2$T$_x$ obtained from the SAED patterns match the ones obtained from XRD (19.8 Å). However, at 21 ± 0.5 Å, the average c for Ti$_3$C$_2$T$_x$-IC measured from the SAED pattern is considerably lower than that obtained from XRD (25 Å). The most probable reason for this state of affairs is the deintercalation of the ammonium species during TEM sample preparation and/or observation (see Methods and Supporting Information section IV).
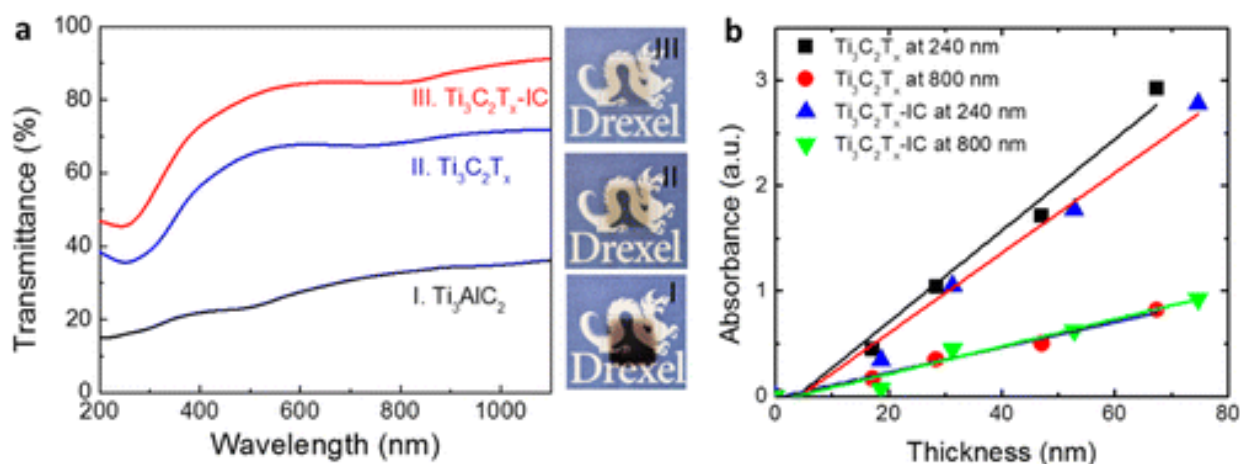
Figure 3. (a) Transmittance spectra and visual images (on right) for (I) Ti_3AlC_2, (II) $Ti_3C_2T_x$, and (III) $Ti_3C_2T_x$-IC films of 15 nm nominal thickness. The films are $\approx 1 \times 1$ cm^2 in area; (b) light absorbance at wavelengths of 240 and 800 nm vs thickness of $Ti_3C_2T_x$ and $Ti_3C_2T_x$-IC films.

The light elements of the surface termination groups (O, H, and F) cannot be seen between the layers, but the larger and nonuniform spacing seen in Figure 2b, c, e, and f indirectly confirm the weak interactions between the MXene layers after etching and the formation of a 2D structure. The nonuniform interlayer spacing observed in the STEM images of the HF-etched sample (Figure 2b) could also account for the peak broadening observed in XRD (Figure 2a).

Prior to etching, the initial thicknesses of the films examined in TEM were 60 nm (Figure 2a). However, as a result of the increase in c and the separation between the MXene layers, due to exfoliation, the etched films were thicker than the initial films (Table 1). Comparing the atomic layers in $Ti_3C_2T_x$-IC (Figure 2c and f) to those of the $Ti_3C_2T_x$ layers (Figures 3b, and e), it is obvious that the former are more uniformly spaced. This result most probably reflects the milder nature of NH_4HF_2 as compared to HF. For the latter, the reaction is faster (Table 1) and more vigorous than the former. Another possible explanation is that the intercalation of ammonia species leads to stronger interactions between MXene layers, essentially "gluing" them together as observed for other MXene intercalation compounds.(22, 30)

In terms of light transmittance, both $Ti_3C_2T_x$ and $Ti_3C_2T_x$-IC films are significantly more transparent than Ti_3AlC_2 of the same initial thickness, 15 nm (Figure 3a, and Table 1). The increased transparency of $Ti_3C_2T_x$ and $Ti_3C_2T_x$-IC, compared to that of Ti_3AlC_2 is also evident visually (Figure 3, middle insets). With 90% transmittance, the $Ti_3C_2T_x$-IC films were the most transparent, followed by the $Ti_3C_2T_x$ films at 70%. With a transmittance of 30%, the Ti_3AlC_2 films were the least transparent. It is worth noting here that the transmittance of all films would have been higher had the TiC incubation layer been absent.

A linear dependence of the absorbance—that is independent of the wavelength of the light—on the thickness of the $Ti_3C_2T_x$ and $Ti_3C_2T_x$-IC films was observed (Figure 3b). Given the similarities in the transmittance curves and the linear dependencies of absorbance values for both samples, it is reasonable to conclude that $Ti_3C_2T_x$ and $Ti_3C_2T_x$-IC are quite similar in structure. A crude estimation of the transmittance of a single MXene layer, d, (since each length c is comprised of two MXene layers, d is approximately equal to the film thickness divided by $2c$) could be obtained from the linear fits of absorbance vs d. The transmittances, calculated at a wavelength of 240 nm, for single layers of $Ti_3C_2T_x$ and $Ti_3C_2T_x$-IC are about 90.5% and 91.5%, respectively; the corresponding transmittances, at a wavelength of 800 nm, are 97.3% and 97.1% respectively. The latter values are quite close to

those reported for graphene single layers.[8] Note that to obtain these values, both the thickness and absorbance of the TiC incubation layer were neglected.

Table 1. Thickness, Etching Duration, Resistivity, and Light Transmittance (at a Wavelength of 700 nm) of the As-Deposited and Etched Ti_3AlC_2 Thin Films

		deposition time [min]	thickness [nm]	etching duration [minutes]	resistivity [μΩm]	transmittance [%]
set 1	Ti_3AlC_2		15.2 ± 0.5[a]		0.45 ± 0.01	31
	$Ti_3C_2T_x$	5	17.2 ± 0.8[a]	9.5	39.23 ± 1.21	68
	$Ti_3C_2T_x$-IC		18.7 ± 0.6[a]	150	4472 ± 323	85
set 2	Ti_3AlC_2		27.7 ± 0.8[a]		0.34 ± 0.01	14
	$Ti_3C_2T_x$	10	28.4 ± 1.8[a]	15	2.28 ± 0.04	49
	$Ti_3C_2T_x$-IC		31.3 ± 1.2[a]	160	5.01 ± 0.03	37
set 3	Ti_3AlC_2		43.4 ± 3.6[b]		0.31 ± 0.01	5.2
	$Ti_3C_2T_x$	20	47.1 ± 3.5[b]	60	22.27 ± 0.43	30
	$Ti_3C_2T_x$-IC		52.8 ± 2.5[b]	420	31 ± 2.8	28
set 4	Ti_3AlC_2		60.0 ± 5.4[c]		0.35 ± 0.01	3.4
	$Ti_3C_2T_x$	30	67.4 ± 5.3[c]	160	1.76 ± 0.02	15
	$Ti_3C_2T_x$-IC		74.7 ± 3.7[d]	660	54 ± 4.51	14

A Determined by XRR (Supporting Information Figure S1a,b).

B Interpolated (Supporting Information Figure S1c).

C Obtained from direct measurement in TEM (Supporting Information Figure S9a for $Ti_3C_2T_x$).

D Obtained from direct measurement in TEM after accounting for the decrease in thickness due to partial deintercalation.

We next turn to the electrical properties, which confirm the metallic-like nature of the conductivities of all etched films despite their optical transparency. As expected, and consistent with previous work,[31] the Ti_3AlC_2 films are metallic with resistivity, ρ, values in the range from 0.37 to 0.45 μΩ m. The latter increase linearly with increasing temperature (Figure 3a). Furthermore, ρ increases with decreasing film thickness (Table 1 and Supporting Information Figure S10). The resistivity values of the $Ti_3C_2T_x$-IC films are systematically higher than those produced by HF etching. For instance, 28 nm nominally thick $Ti_3C_2T_x$ and $Ti_3C_2T_x$-IC films have ρ values of 2.3 and 5.0 μΩ m, respectively. This result is also consistent with previous work that has shown that intercalation of MXenes with organic compounds increases their resistivity.[30] The resistivities of the etched films also depend significantly on etching time; longer etching times lead to higher ρ values presumably due to the formation of defects (see Supporting Information Table S2), in agreement with previous work.[32] The results listed in Table 1 are those obtained upon the full MAX to MXene conversion. The latter was determined by intermittently etching each film, followed by XRD. When the Ti_3AlC_2 peaks disappeared, the etching process was halted (Supporting Information Figure S6). We note in passing that there were no changes in the *c* lattice parameter with etching time. Furthermore, the fact that the conductivities are affected by the intercalants, suggests that MXenes can potentially be used as sensors.

At 1.8 μΩ m, a 60 nm nominally thick $Ti_3C_2T_x$ sample is the most conductive of the HF etched films $Ti_3C_2T_x$ films (Table 1). However, at 700 nm wavelength, its transmittance is only 15%. The 15 nm nominally thick $Ti_3C_2T_x$ sample exhibited the highest transmittance (68% at 700 nm wavelength) with a ρ of 39.2 μΩ m. For the $Ti_3C_2T_x$-IC films, the lowest resistivity was 5.0 μΩ m, with a transmittance of about 37%; the most transparent (>85% at 700 nm wavelength) had a resistivity of ≈4.5 mΩ m.

At this juncture, it is worth comparing our results with other conductive electrodes at a wavelength of 550 nm. Referring to Supporting Information Figure S10, it is obvious that while the transmittance of our thinnest films is higher than that of indium tin oxide, ITO, their sheet resistance values are orders of magnitude higher. When compared to graphene transparent conductive electrodes, again MXene transmittance values are slightly higher, but the resistivity is about 2 orders of magnitude higher.

Why the resistivities measured herein are as high as they are, is unclear at this time. One possibility is the film morphology. As noted above, the Ti_3AlC_2 films are predominantly *c*-axis oriented (Figure 2a). However, a secondary grain population, whose basal planes are not parallel to the substrate, also exists (see Supporting Information Figure S9). If the reasonable assumption is made that after etching the conductivity along [0001] is significantly lower than along [100], this secondary grain population, will act as insulating islands. Reducing the fraction of such grains should result in films that are more conductive when etched. Deintercalation of films by heat treatment can alone increase the conductivity by an order of magnitude or more.(30)

Theoretical calculations predict that it is possible to alter the electronic properties of MXenes by altering their surface terminations.(21, 33) For example, pure Ti_3C_2 is predicted to exhibit a metallic behavior, whereas $Ti_3C_2F_2$ and $Ti_3C_2(OH)_2$ are predicted to have band gaps of 0.05 and 0.1 eV, respectively.(4, 13) Thus, another potential avenue for enhancing the films' conductivities is to eliminate the surface groups. We note in passing that several applications, such as touch screen, electromagnetic shielding for cathode ray tubes and electrostatic dissipation, require sheet resistance values which are comparable to what we report for MXene thin films, viz. 1000 to 1 MΩ/sq.(34)

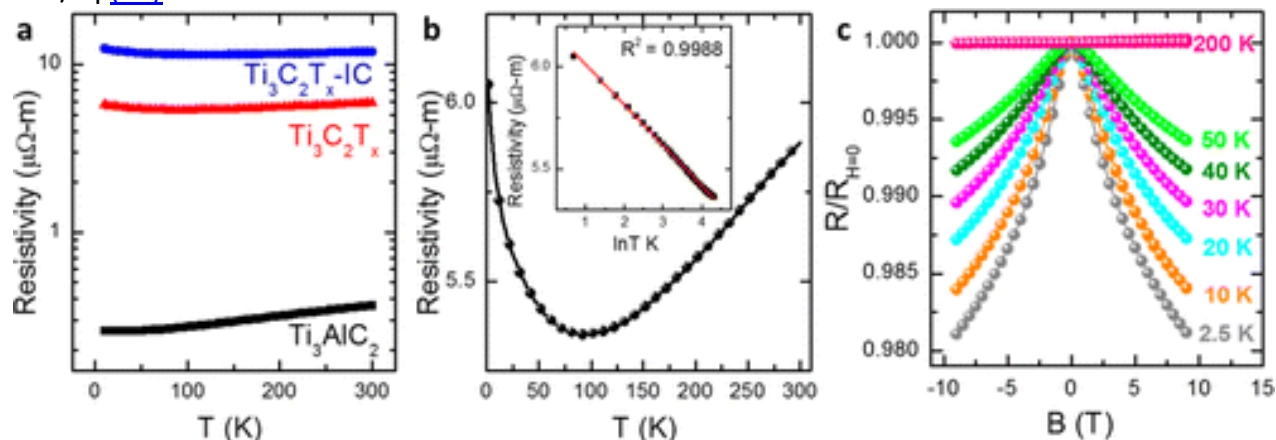**Figure 4.** Dependence of the electrical behavior of Ti_3AlC_2, $Ti_3C_2T_x$, and $Ti_3C_2T_x$-IC films on temperature and magnetic field. (a) Resistivity vs temperature for Ti_3AlC_2, $Ti_3C_2T_x$, and $Ti_3C_2T_x$–IC films of 20 nm nominal thickness. (b) Resistivity vs temperature for $Ti_3C_2T_x$ of 28 nm nominal thickness. Inset shows fitting of resistivity, over the temperature range of 2 to 74 K, to the weak localization model (ρ ~ ln T). (c) Comparison of normalized magnetoresistance curves for $Ti_3C_2T_x$ of 28 nm nominal thickness at various temperatures ranging from 2.5 to 200 K. $R_{H=0}$ refers to the film resistance in the absence of applied magnetic field.

To elucidate the conduction mechanisms of the MXene layers, their resistivities, and magnetoresistances (MRs) from room temperature down to about 2.5 K were measured. Figure 4a shows the temperature dependent resistivity for Ti_3AlC_2, $Ti_3C_2T_x$, and $Ti_3C_2T_x$-IC films of 28 nm nominal thickness. The Ti_3AlC_2 films exhibit metallic behavior from 300 K down to about 10 K. For the $Ti_3C_2T_x$ and $Ti_3C_2T_x$-IC films, on the other hand, metallic behavior is observed from 300 to about 100 K; below 100 K the resistivity increases with decreasing temperature (Figure 4b). Similar low-temperature behavior was observed in other $Ti_3C_2T_x$ and $Ti_3C_2T_x$-IC films (see Supporting Information Figure S11). The low temperature transport data can best be fit assuming $\rho \sim \ln T$ (inset in Figure 4b). As shown in Supporting Information Figure S7, other mechanisms associated with insulating behavior, such as thermally activated processes, 3D variable range hopping and others, do not accurately reflect the ρ (T) data (see Supporting Information Figure S12). The logarithmic dependence on temperature is consistent with weak localization, a phenomenon caused by electron backscattering and often observed in 2D metals.[35] To provide further insight into the transport properties, MR measurements were performed in the low temperature ($d\rho/dT < 0$) and high temperature ($d\rho/dT > 0$) regimes. The appearance of negative MR in the low temperature regime (Figure 4c) is again consistent with weak localization, verifying that these materials are indeed 2D.[35-37]

Conclusions

In conclusion, epitaxial $Ti_3C_2T_x$ films can be readily produced by the room temperature etching of epitaxial Ti_3AlC_2 thin films in HF or NH_4HF_2 solutions. The latter etchant yields films intercalated with NH_3 and NH_4^+ species, that have c lattice parameters (~ 25 Å) that are 25% larger than films etched with HF. The $Ti_3C_2T_x$-IC films have higher transparencies and resistivities than their $Ti_3C_2T_x$ counterparts. $Ti_3C_2T_x$ and $Ti_3C_2T_x$-IC films of $\sim$15-nm nominal thickness were found to be 68 and 85% transparent, respectively. Both films also exhibited metallic conductivity down to 100 K; below 100 K, the resistivities increase with decreasing temperatures and exhibit negative MRs at the lowest temperatures, both attributes consistent with, and evidence for, their 2D metallic nature.

The MXene films produced herein are promising materials for transparent conductive electrodes, sensors and other applications. By better control of the deposition process, such that nonbasal growth is eliminated or minimized, the potential exists for enhancing their conductivities. A parallel approach is to modify, or eliminate, the surface terminations such as F, O, or OH.

Synthesis of single-layer Ti_3C_2 films is the next frontier. Other MXenes (Ti-based and others containing other transition metals such as Nb, V, Ta, etc. or nitrogen in addition to carbon) may also show attractive optical and electrical properties and should be produced and studied in their thin-film state. It is vital to note here that the production of epitaxial uniform multilayer MXene films is a necessary and crucial first step to applying this novel and unique family of materials in the field of electronics, optoelectronics and photonics. Given the vast richness of MXene chemistries, together with the multiple different intercalants (from cations to polymers to organic molecules), it is obvious that we are standing at the edge of a truly vast *terra incognita*.

Supporting Information

XRR, thickness determination, XPS analysis of Ti_3AlC_2, $Ti_3C_2T_x$ and $Ti_3C_2T_x$-IC thin films, XRD analysis of byproducts from etching Ti_3AlC_2 with NH_4HF_2, intercalation and deintercalation of $Ti_3C_2T_x$ thin films, optimization of the etching process, EDX mapping of $Ti_3C_2T_x$, SEM and TEM for Ti_3AlC_2 and

$Ti_3C_2T_x$ thin films, and electrical transport measurements and analysis. This material is available free of charge via the Internet at http://pubs.acs.org.

Author Contributions

Acknowledgment

References

This article references 40 other publications.

1. Novoselov, K. S.; Geim, A. K.; Morozov, S. V.; Jiang, D.; Zhang, Y.; Dubonos, S. V.; Grigorieva, I. V.; Firsov, A. A. Science 2004, 306, 666– 669

[CrossRef], [PubMed], [CAS]

2. Novoselov, K.; Jiang, D.; Schedin, F.; Booth, T.; Khotkevich, V.; Morozov, S.; Geim, A. Proc. Natl. Acad. Sci. U.S.A. 2005, 102, 10451– 10453

[CrossRef], [PubMed], [CAS]

3. Novoselov, K. S.; Fal'ko, V. I.; Colombo, L.; Gellert, P. R.; Schwab, M. G.; Kim, K.A Roadmap for Graphene Nature 2012, 490, 192– 200

[CrossRef], [PubMed], [CAS]

4. Tang, Q.; Zhou, Z. Progress in Materials Science 2013, 58.

[CrossRef]

5. Nicolosi, V.; Chhowalla, M.; Kanatzidis, M. G.; Strano, M. S.; Coleman, J. N. Science 2013, 340, 1420– 1438

[CrossRef], [CAS]

6. Zhang, X.; Xie, Y. Chem. Soc. Rev. 2013, 42, 8187– 8199

[CrossRef], [PubMed], [CAS]

7. Bolotin, K. I.; Sikes, K. J.; Jiang, Z.; Klima, M.; Fudenberg, G.; Hone, J.; Kim, P.; Stormer, H. L. Solid State Commun. 2008, 146, 351– 355

[CrossRef], [CAS]

8. Nair, R. R.; Blake, P.; Grigorenko, A. N.; Novoselov, K. S.; Booth, T. J.; Stauber, T.; Peres, N. M.; Geim, A. K. Science 2008, 320, 1308

[CrossRef], [PubMed], [CAS]

9. Ci, L.; Song, L.; Jin, C.; Jariwala, D.; Wu, D.; Li, Y.; Srivastava, A.; Wang, Z. F.; Storr, K.; Balicas, L.; Liu, F.; Ajayan, P. M. Nat. Mater. 2010, 9, 430– 435

[CrossRef], [PubMed], [CAS]

10. van der Zande, A. M.; Huang, P. Y.; Chenet, D. A.; Berkelbach, T. C.; You, Y.; Lee, G. H.; Heinz, T. F.; Reichman, D. R.; Muller, D. A.; Hone, J. C. Nat. Mater. 2013, 12, 554– 561

[CrossRef], [PubMed], [CAS]

11. Najmaei, S.; Liu, Z.; Zhou, W.; Zou, X.; Shi, G.; Lei, S.; Yakobson, B. I.; Idrobo, J. C.; Ajayan, P. M.; Lou, J. Nat. Mater. 2013, 12, 754– 759

[CrossRef], [PubMed], [CAS]

12. Naguib, M.; Mochalin, V. N.; Barsoum, M. W.; Gogotsi, Y. Adv. Mater. 2014, 26, 992– 1005

[CrossRef], [CAS]

13. Naguib, M.; Kurtoglu, M.; Presser, V.; Lu, J.; Niu, J.; Heon, M.; Hultman, L.; Gogotsi, Y.; Barsoum, M. W. Adv. Mater. 2011, 23, 4248– 4253

[CrossRef], [CAS]

14. Barsoum, M. W. MAX Phases: Properties of Machinable Ternary Carbides and Nitrides; John Wiley & Sons: New York, 2013.

[CrossRef]

15. Naguib, M.; Mashtalir, O.; Carle, J.; Presser, V.; Lu, J.; Hultman, L.; Gogotsi, Y.; Barsoum, M. W. ACS Nano 2012, 6, 1322– 1331

[ACS Full Text], [PubMed], [CAS]

16. Naguib, M.; Halim, J.; Lu, J.; Cook, K. M.; Hultman, L.; Gogotsi, Y.; Barsoum, M. W. J. Am. Chem. Soc. 2013, 135, 15966– 15969

[ACS Full Text], [PubMed], [CAS]

17. Enyashin, A.; Ivanovskii, A. J. Solid State Chem. 2013, 207, 42– 48

[CrossRef], [CAS]

18. Enyashin, A. N.; Ivanovskii, A. L. J. Phys. Chem. C 2013, 117, 13637– 13643

[ACS Full Text], [CAS]

19. Naguib, M.; Come, J.; Dyatkin, B.; Presser, V.; Taberna, P. L.; Simon, P.; Barsoum, M. W.; Gogotsi, Y. Electrochem. Commun. 2012, 16, 61– 64

[CrossRef], [CAS]

20. Tang, Q.; Zhou, Z.; Shen, P. J. Am. Chem. Soc. 2012, 134, 16909– 16916

[ACS Full Text], [PubMed], [CAS]

21. Shein, I. R.; Ivanovskii, A. L. Micro Nano Lett. 2013, 8, 59– 62

[CrossRef], [CAS]

22. Lukatskaya, M. R.; Mashtalir, O.; Ren, C. E.; Dall'Agnese, Y.; Rozier, P.; Taberna, P. L.; Naguib, M.; Simon, P.; Barsoum, M. W.; Gogotsi, Y. Science 2013, 341, 1502– 1505

[CrossRef], [PubMed], [CAS]

23. Misra, A.; Prasad, J.; Sees, J. A.; Hall, L. H. Benign Method for Etching Silicon Dioxide. U.S. Patent No. 6048406, 2000.

24. Bourbigot, S.; Le Bras, M.; Gengembre, L.; Delobel, R. Appl. Surf. Sci. 1994, 81, 299– 307

[CrossRef], [CAS]

25. Egawa, C.; Naito, S.; Tamaru, K. Surf. Sci. 1983, 131, 49– 60

[CrossRef], [CAS]

26. Rakov, E. G. e.; Mel'nichenko, E. Russ. Chem. Rev. 1984, 53, 851– 869

[CrossRef]

27. Friend, R. H.; Yoffe, A. D. Adv. Phys. 1987, 36, 1– 94

[CrossRef], [CAS]

28. Bernard, L.; Mckelvy, M.; Glaunsinger, W.; Colombet, P. Solid State Ionics 1985, 15, 301– 310

[CrossRef], [CAS]

29. Wilhelmsson, O.; Palmquist, J.-P.; Lewin, E.; Emmerlich, J.; Eklund, P.; Persson, P.; Högberg, H.; Li, S.; Ahuja, R.; Eriksson, O. J. Cryst. Growth 2006, 291, 290– 300

[CrossRef], [CAS]

30. Mashtalir, O.; Naguib, M.; Mochalin, V. N.; Dall'Agnese, Y.; Heon, M.; Barsoum, M. W.; Gogotsi, Y. Nat. Commun. 2013, 4, 1716

[CrossRef], [CAS]

31. Wilhelmsson, O.; Palmquist, J.-P.; Nyberg, T.; Jansson, U. Appl. Phys. Lett. 2004, 85, 1066– 1068

[CrossRef], [CAS]

32. Mashtalir, O.; Naguib, M.; Dyatkin, B.; Gogotsi, Y.; Barsoum, M. W. Mater. Chem. Phys. 2013, 139, 147– 152

[CrossRef], [CAS]

33. Khazaei, M.; Arai, M.; Sasaki, T.; Chung, C. Y.; Venkataramanan, N. S.; Estili, M.; Sakka, Y.; Kawazoe, Y. Adv. Funct. Mater. 2013, 23, 2185– 2192

[CrossRef], [CAS]

34. Geng, H.-Z.; Kim, K. K.; So, K. P.; Lee, Y. S.; Chang, Y.; Lee, Y. H. J. Am. Chem. Soc. 2007, 129, 7758– 7759

[ACS Full Text], [PubMed], [CAS]

35. Bergmann, G. Phys Rev B 1982, 25, 2937– 2939

[CrossRef], [CAS]

36. Bergmann, G. Phys. Rep. 1984, 107, 1– 58

[CrossRef], [CAS]

37. Henzler, M.; Lüer, T.; Heitmann, J. Phys Rev B 1999, 59, 2383– 2387

[CrossRef], [CAS]

38. Emmerlich, J.; Högberg, H.; Sasvári, S.; Persson, P. O. Å.; Hultman, L.; Palmquist, J.-P.; Jansson, U.; Molina-Aldareguia, J. M.; Czigány, Z. J. Appl. Phys. 2004, 96, 4817– 4826

[CrossRef], [CAS]

39. Frodelius, J.; Eklund, P.; Beckers, M.; Persson, P.; Högberg, H.; Hultman, L. Thin Solid Films 2010, 518, 1621– 1626

[CrossRef], [CAS]

40. Eklund, P.; Beckers, M.; Frodelius, J.; Högberg, H.; Hultman, L. J. Vac. Sci. Technol., A 2007, 25, 1381– 1388

[CrossRef], [CAS]